

TURBULENT TRANSPORT IN ROCKET MOTOR UNSTEADY FLOWFIELD

Weidong Cai and V. Yang
The Pennsylvania State University
University Park, Pennsylvania

G. A. Flandro
University of Tennessee Space Institute
Tullahoma Tennessee

Abstract

This paper describes an approximate method for estimating effects of turbulence on the unsteady flowfield and on the stability of wave motions in a solid propellant rocket chamber. Recent work has illuminated the laminar features of this problem. The objective of the present work is to determine in a simplified way some of the effects of turbulence on these processes. A fundamental question to be answered is whether or not the presence of fully developed turbulence modifies the linearized stability integrals (e.g. flow-turning) that arise naturally in the laminar analysis. The problem is treated by combining realistic numerical solutions for the turbulent field with detailed analytical solutions for the organized oscillatory gas motions. The main influence of turbulence is modification of the transport properties and the mean chamber velocity profile. The results show that the organized vorticity waves that fill the entire chamber in the laminar case reduce to a thin acoustic boundary layer in the presence of strong turbulence. From the standpoint of vorticity production, this can be viewed as a transition from organized vorticity associated with the periodic wave structure to the wideband vorticity distribution of the turbulent field. This process is similar in many respects to the turbulent transition process in a flow without organized oscillations. In that case organized oscillations (e.g. Tollmein-Schlichting waves) appear naturally as an intermediate stage in the transition to a fully turbulent field. Despite the major impact of turbulence on the flow geometry, there is little change in linear acoustic stability gain/loss terms related to vorticity propagation. This reinforces the concept that the flow-turning interaction is not the result of viscous losses at the chamber boundaries. However, it is clear that stochastic fluctuations can have a major influence on the flame zone dynamic behavior especially in the nozzle end of a long motor burning port where the flow becomes fully turbulent.

Introduction

Recent work by several investigators using both analytical and numerical methods has revealed some of the details of the rotational flow effects of importance in rocket combustion instability. Although analytical studies have heretofore been limited to laminar treatment of the unsteady viscous flowfield, they have yielded useful information needed in accurate motor stability assessment. In particular, they have revealed the origin of the flow-turning loss mechanism and other potentially important additions to the system energy gain/loss balance. Numerical solution of similar unsteady flows have verified these analytical solutions in laminar

regions of the chamber but indicate that the transition to turbulence markedly influences the results. The purpose of this research is to utilize information from the numerical calculations in extending the analytical results into the turbulent regime. There are several motives for doing this. Apart from the obvious benefit of enhanced physical understanding inherent in analytical models for complicated flow fields such as those in an unstable rocket chamber, there remain many practical questions related to the precise manner in which turbulent flow processes affect the stability computations.

An approximate method for including the turbulence effects is described. The field is decomposed into two elements. The first is a realistic numerical model of the mean flow which includes the corrections to the transport properties resulting from transition and growth of random turbulent eddies. The second is a detailed analytical model of organized unsteady motion consisting of the acoustic field and associated rotational waves created by production of vorticity at the chamber inflow boundaries. Information on the mean flow with turbulence is obtained from a detailed computational model by Yang and his coworkers¹. This provides spatial distributions of the turbulence-modified flow field and associated transport properties. These are then employed in the analytical flowfield expressions to produce the corrected unsteady field. This procedure is approximate in that the direct interaction between the organized and turbulent fluctuations is neglected. It is believed that in most cases these are not strong interactions, so the main effect of turbulence on the organized oscillations comes from the changes in transport properties and the mean flow velocity distribution.

Results compare favorably to the complete unsteady simulations¹. In particular, as the nozzle end of the chamber is approached, the turbulence effects grow rapidly in importance. The organized vortical waves are more rapidly damped due mainly to increase in the effective coefficient of viscosity (eddy viscosity), and the motion can then truly be described as an acoustic boundary layer; the organized rotational effects are confined to a thin region near the burning surface. The unsteady vorticity distribution outside this boundary layer does not then contain components directly related to the irrotational acoustic field. Despite this major departure for the laminar description of the unsteady rotational flow, there is little change in the basic effects of vorticity production on the system stability characteristics. That is, important contributions to the system energy gain/loss balance such as the flow-turning loss are not strongly affected by turbulence. Direct interactions of the turbulent field with the combustion processes near the propellant are not considered in the present effort, but will be incorporated in developing flame zone models.

Analysis

An irrotational (acoustic) unsteady flow is not a sufficiently complete model of the unsteady combustion chamber gas motion. Such a model allows slip flow at the propellant surfaces. Acoustic boundary layer theory, which has been applied to this problem frequently in the past, may not be appropriate since the strong convective field in the chamber transports vorticity throughout the domain. Such motion may be laminar near the forward end of the chamber but will naturally transition to fully turbulent motion downstream. It is necessary to determine the effect of this turbulence on the organized wave motion in order that a realistic assessment of combustion instability can be carried out. In particular it is required to determine the effects of modifications to the transport properties and mean flow geometry introduced by transition to a fully turbulent flow.

It is not clear at the outset what role, if any, is played by viscosity since the radial convection tends to discourage formation of highly sheared regions of flow. It is also important to realize that the creation of vorticity does not require the presence of viscous stresses. Crocco's theorem¹⁴ clarifies the origin of both the steady and unsteady vorticity in the gas particles entering the chamber from the burning zone.

The analysis is carried out in two parts. In the first, a realistic model of the effects of turbulence on the mean flow field in the rocket chamber is described; numerical results based on this model give the turbulent transport properties needed in assessing the analytical model of the unsteady motion carried out in the second part.

Mean Flow Field with Turbulence

The formulation of the mean flow field is based on the conservation equations of mass, momentum and energy. Full account is taken of variations of thermophysical properties. In vector notation, the governing equations in two-dimensional Cartesian coordinates can be written in the following conservative form:

$$\frac{\partial \mathbf{Q}}{\partial t} + \frac{\partial}{\partial x}(\mathbf{E} - \mathbf{E}_V) + \frac{\partial}{\partial y}(\mathbf{F} - \mathbf{F}_V) = \mathbf{S} \quad (1)$$

Definitions of the variable vector \mathbf{Q} , the convective flux vectors \mathbf{E} and \mathbf{F} , the diffusive flux vectors, \mathbf{E}_V and \mathbf{F}_V and the source vector \mathbf{S} , can be found in Reference 1.

The k - ε model is used to achieve turbulence closure. In order to account for the wall damping effect on turbulence, a two-layer turbulence model suggested by Rodi (Ref. 2) is employed. In this approach, the standard k - ε model is applied to regions away from the wall and a one-equation model is implemented close to the wall. Description of the standard k - ε model can be found in Reference 3. In the inner layer, the ε -equation described above fails since viscous effects are dominant. Only the k -equation is invoked in this region. In order to achieve turbulence closure, a turbulence length scale is empirically introduced to evaluate the turbulence dissipation rate and eddy viscosity. Unlike the treatment of high Reynolds number flows, Rodi² proposed two different turbulence length scales, namely, turbulence dissipation length scale l_ε for quantifying the turbulence dissipation rate, and the turbulence viscosity length scale l_u for evaluating eddy viscosity. These two length scales are simulated in a manner similar to the vanDriest damping function used in the mixing length model:

$$l_u = c_1 y \left[1 - \exp \left(- \frac{Re_y}{A_u} \frac{25}{A^+} \right) \right] \quad (2)$$

$$l_\varepsilon = c_1 y \left[1 - \exp \left(- \frac{Re_y}{A_\varepsilon} \right) \right] \quad (3)$$

where $Re_y = k^{1/2} y / \nu$ is the local Reynolds number, and the constants A_u and A_ε are 70 and 5.08, respectively. In conformity with the logarithmic law, the constant c_1 is set equal to κ being the vonKarman constant.

Two modifications are applied to account for the effects of wall transpiration and flow unsteadiness. As several experimental researchers^{4,5,6} observed, turbulence intensity and velocity fluctuations increase with increasing mass injection rate near the wall, as well as does the Reynolds shear stress. Surface mass injection tends to reduce the wall damping effect, and the turbulence length scale is less damped by the wall with increasing injection rate. In the

present work, the model modification is based on Kay's experimental work,⁶ which follows directly the concepts developed for the mixing length model. Kay argued that the mixing length is effectively equal to the turbulence length scale. Following the form of the van Driest damping function, A^+ in Eq.(2) is modified by considering the wall injection and pressure gradient effects.

$$A^+ = \frac{A_0^+}{5.51 \left[v_w^+ + \frac{5.86P^+}{(1 + 5.0v_w^+)} \right] + 1.0} \quad (4)$$

where A_0^+ is the value of A^+ under conditions without wall transpiration and pressure gradient, and $v_w^+ = v_w / u_\tau$. The influence of pressure gradient is taken into account by introducing $P^+ = -K^{3/2}(C_f / 2)^{2/3}$ where $K = v / U_\infty^2 (dU_\infty / dx)$. This approach was first implemented in Tseng's work with great success.⁷

A variety of experiments have been performed to study turbulence intensity in unsteady flows. Cousteix et al.⁸ reached the following conclusion in the study of turbulent boundary layers with external oscillations. Although the measured turbulence intensity and Reynolds shear stress in various parts may change, the ratio of the shear stress to its component turbulence intensities remains constant at a value equivalent to that of steady flow. Thus, under certain circumstances, such as the oscillation frequency not being too high, a steady flow turbulence model may be used to predict unsteady turbulence behavior. However, it is highly possible that substantial changes in turbulence intensity may occur. As the oscillation frequency increases, a critical value (unfortunately, this value is not available at the present time due to limited experimental and theoretical studies) can be reached above where significant interactions between oscillatory motions and turbulence structure may occur. Experimental studies by Mizushima⁹ and Ramaprian and Tu¹⁰ have proven this phenomenon. Another noticeable feature is related to the turbulence modeling for unsteady flows. When an external oscillating velocity is imposed on a viscous flow, the flow near the wall responds quite readily to this unsteadiness. In many of the experiments that have been performed, the unsteady viscous reaction to the imposed flow variation is almost confined to the Stokes layer near the wall; the outer region of the boundary layer behaves not as alert as the inner layer. This is very important to researchers whose focus is on the characteristics near the wall. Model modifications, especially near the wall, become necessary. In their study of the performance of low-Reynolds-number turbulence models for unsteady boundary layers without wall transpiration, Fan and Lakshminarayana¹¹ pointed out that an instantaneous logarithmic law does not generally exist in the near-wall region, and two treatments may be considered because of the rapid change in the phases of the flow quantities: (1) the local turbulence characteristic velocity or local Reynolds number, instead of inner variable y^+ should be used in the formulation of near-wall and low-Reynolds-number functions; and (2) a more stringent requirement on near-wall and low-Reynolds-number functions for the asymptotic behavior of turbulence quantities is necessary. Although only the turbulence length scales need to be modified, these ideas may be useful in the present two-layer model, such as the use of the local turbulent Reynolds number as a correlation parameter to evaluate the turbulent length scale embodied in Eq.(2) and Eq.(3). Kovalnogov¹² studied experimentally heat transfer and friction in unsteady turbulent flows with a longitudinal pressure gradient in a chamber. The velocity transient and longitudinal

pressure gradient exert an indirect effect by changing the coefficients of turbulent momentum transfer in the flow. This effect can be taken into account by modifying the turbulence length scale:

$$\frac{1}{l_0} = \left[1 + C_1 \frac{\frac{\partial u_\infty}{\partial t} + u_\infty \frac{\partial u_\infty}{\partial x}}{u_{0\infty} \left(\frac{\partial u}{\partial y} \right)_{y=0}} \right] \quad (5)$$

where l_0 is the turbulence length scale in a steady flow. The subscript ∞ refers to the free stream condition and the subscript 0∞ to the chamber inlet condition. A numerical value of 21.4 was found for C_1 in Kovalnogov's experimental work. In the present study, there is no inlet velocity since the head end of the chamber is closed. Thus, $u_{0\infty}$ is chosen as the average velocity of local section area:

$$u_{0\infty} = \frac{1}{A} \int u dA. \quad (6)$$

Formulation of Unsteady Viscous Flow Model

Much of the literature describing the evolution of oscillatory flow in a rocket chamber is based on the assumption of acoustic waves. That is, the time-dependent field is taken to be irrotational. In order to incorporate turbulence effects it is necessary to incorporate fully the rotational flow effects including all viscous terms in the unsteady formulation. A method based on that described in Reference 14 will be used. However, modifications must be made to explicitly include both the effects of the eddy viscosity and the spatial variability of the viscosity and other mean transport properties. As already described, it is anticipated that a main effect of turbulence will be the modification of the transport properties and thus there will likely be large variations in local values.

The standard assumptions and nomenclature used in combustion stability modeling are employed here for convenience in interpreting the results. Velocities are made dimensionless with respect to the chamber sound speed, a_0 , to emphasize the central role of compressibility in the oscillating field. Lengths are referenced to the chamber radius, R ; the acoustic wavelength expressions then contain the chamber length-to-radius ratio since longitudinal oscillations will be of primary concern. Time is made dimensionless by dividing by the characteristic time represented by the ratio R/a_0 . Pressure is normalized by γP_0 and other thermodynamic variables are nondimensionalized with respect to their respective chamber stagnation properties. \mathbf{U} is the mean flow velocity vector. Either a laminar or turbulent form for the mean flow must be accommodated depending on the location within the chamber.

The momentum balance for the first-order unsteady viscous flow is

$$\frac{\partial \mathbf{u}^{(1)}}{\partial t} + \nabla p^{(1)} = -M_b \left[\begin{array}{l} \nabla(\mathbf{u}^{(1)} \cdot \mathbf{U}) - \mathbf{u}^{(1)} \times \nabla \times \mathbf{U} - \\ -\mathbf{U} \times \nabla \times \mathbf{u}^{(1)} \end{array} \right] + \left[\begin{array}{l} -\nabla \times \nabla \times \delta^2 \mathbf{u}^{(1)} + \nabla(\mathbf{u}^{(1)} \cdot \nabla \delta^2) \\ + \frac{4}{3} \nabla(\delta^2 \nabla \cdot \mathbf{u}^{(1)}) - \mathbf{u}^{(1)} \nabla^2 \delta^2 + \\ + \nabla \delta^2 \times \nabla \times \mathbf{u}^{(1)} - \nabla \delta^2 \nabla \cdot \mathbf{u}^{(1)} \end{array} \right] \quad (7)$$

where superscript (1) indicates that terms of first-order in wave amplitude are retained. The first group of terms on the right represents the convective interactions between the mean flow and the oscillatory field. These will be handled as perturbations on the organized fluctuations since they are proportional to the mean flow Mach number at the burning surface, M_b , which is used as a second small parameter in the mathematical strategy. Viscous effects, the second set of terms on the right of Eq. (7), are represented in dimensionless form in terms of the inverse of the Reynolds number, δ^2 , based on the chamber size and the sound speed:

$$\delta = \delta(\mathbf{r}) = \sqrt{\frac{\nu}{a_0 R}} \quad (8)$$

which must be treated as a function of position since the kinematic viscosity coefficient, ν , consists of contributions from both molecular and turbulent diffusion. The turbulent component varies strongly with position. Values for ν and its derivatives must be obtained from the numerical turbulent mean flow calculations.

Conservation of mass requires that

$$\frac{\partial p^{(1)}}{\partial t} + \nabla \cdot \mathbf{u}^{(1)} = -M_b \mathbf{U} \cdot \nabla p^{(1)} \quad (9)$$

Assuming sinusoidal oscillations, $p^{(1)} = p' \exp(-ik_m t)$ and $\mathbf{u}^{(1)} = \mathbf{u}' \exp(-ik_m t)$ where primes denote the complex amplitudes, the equation for the unsteady vorticity amplitude, $\boldsymbol{\omega}' = \nabla \times \mathbf{u}'$, is found by taking the curl of Eq. (7) with the result

$$ik_m \boldsymbol{\omega}' = -M_b \nabla \times [\mathbf{u}' \times \boldsymbol{\Omega} + \mathbf{U} \times \boldsymbol{\omega}'] - \nabla \times \left[\begin{array}{l} -\nabla \times \nabla \times \delta^2 \mathbf{u}' - \mathbf{u}' \nabla^2 \delta^2 + \\ + \nabla \delta^2 \times \boldsymbol{\omega}' - \nabla \delta^2 \nabla \cdot \mathbf{u}' \end{array} \right] \quad (10)$$

In the present application to a cylindrical geometry with burning at the sidewall and an axial acoustic wave, the vorticity vector has only an azimuthal component.

The boundary condition that must be satisfied by the vorticity at the burning surface is found by evaluating the axial component of Eq. (7) at $r = 1$ and solving for terms involving the vorticity amplitude. One finds that

$$\boldsymbol{\omega}' + \frac{\delta^2}{M_b} \left[\frac{\partial \boldsymbol{\omega}'}{\partial r} + \left(1 + \frac{1}{\delta^2} \frac{\partial \delta^2}{\partial r} \right) \boldsymbol{\omega}' \right] = -\frac{1}{M_b} \frac{\partial p'}{\partial z} \quad (11)$$

at the burning surface. The no-slip condition has been applied. Several terms in the axial momentum balance are not shown because they are several orders of magnitude smaller than the term representing the effect of the axial pressure gradient. This indicates that the vorticity production at the surface is primarily due to the axial unsteady pressure gradient across the incoming mean flow streamlines. When turbulence from the main flow stream penetrates to the vicinity of the surface, it is likely that viscous stresses are enhanced because of the modified transport properties. Then the second group of terms on the left of Eq. (4) will play an important role in setting the boundary condition for the organized unsteady vorticity. It is necessary to carefully retain them in the problem solution. At the surface, the scaling parameter δ^2/M_b is the inverse of the injection Reynolds number,

$$R_i = \frac{M_b}{\delta^2} = \frac{v_b R}{v}$$

It may be either very small in the laminar case and significantly larger if fully turbulent conditions are present near the injection surface.

It is useful to distinguish between rotational and irrotational parts of the velocity field. The latter part will represent the acoustic motions which are not strongly affected in a direct manner by viscous effects. The superimposed rotational part is associated with vorticity production at the boundary and accounts for the viscous interactions as well as the direct connection to the turbulent fluctuations. Thus, to represent the unsteady velocity as a combination of irrotational and rotational parts, put

$$\mathbf{u}' = \hat{\mathbf{u}} + \tilde{\mathbf{u}} \quad (12)$$

where the circumflex ($\hat{\mathbf{u}}$) indicates the acoustic (irrotational) part whereas the tilde ($\tilde{\mathbf{u}}$) identifies the rotational component.

For a three-dimensional cylindrical chamber, the axial acoustic motion representing longitudinal gas oscillations is the simple plane wave solution

$$\begin{cases} p' = \cos(k_m z) \\ \hat{\mathbf{u}} = \hat{w} \mathbf{e}_z = i \sin(k_m z) \mathbf{e}_z \end{cases} \quad (13)$$

This solution will be utilized to enable simple assessment of the new turbulence corrections by direct comparison to previous analyses that utilize this base representation for the chamber oscillations.

Unsteady Vorticity

In order to determine the correct form for the rotational unsteady velocity, $\tilde{\mathbf{u}}$, it is first necessary to solve for the unsteady vorticity from Eq. (10) subject to the boundary condition of Eq. (11), which, as has already been noted is the equivalent of the no-slip condition. Once ω' is known, the momentum and continuity balances, Eqs. (7) and (9) can be solved for the rotational velocity vector. For the assumed cylindrical geometry, Eq. (10) is

$$ik_m \omega' - M_b \left(U_r \frac{\partial \omega'}{\partial r} + U_z \frac{\partial \omega'}{\partial z} - \frac{U_r}{r} \omega' \right) = \left\{ \begin{array}{l} -\delta^2 \left(\frac{\partial^2 \omega}{\partial r^2} + \frac{1}{r} \frac{\partial \omega}{\partial r} - \frac{\omega}{r^2} + \frac{\partial^2 \omega'}{\partial z^2} \right) + \\ + \frac{\partial \delta^2}{\partial z} \left(\frac{4}{3} \frac{\partial \omega'}{\partial z} - \frac{\partial \omega'}{\partial r} \right) - \frac{\partial \delta^2}{\partial r} \left(r \frac{\partial \omega'}{\partial r} + \frac{\omega'}{r} \right) \\ - \frac{\partial^2 \delta^2}{\partial r \partial z} \omega' + \frac{\partial^2 \delta^2}{\partial z^2} \omega' + \\ + M_b \left[\Omega \left(ik_m p' - \frac{u'}{r} \right) + u' \frac{\partial \Omega}{\partial r} + w' \frac{\partial \Omega}{\partial z} \right] \end{array} \right\} \quad (14)$$

Though linear, this equation is difficult to solve due primarily to the variable coefficients representing the steady velocity components and vorticity, Ω . The latter can be represented in the laminar part of the chamber by the Culick mean flow model as

$$\left\{ \begin{array}{l} U_r = -\sin\left(\frac{1}{2}\pi r^2\right)/r \\ U_z = \pi z \cos\left(\frac{1}{2}\pi r^2\right) \\ \Omega = \pi^2 z r \sin\left(\frac{1}{2}\pi r^2\right) \end{array} \right. \quad (15)$$

$$\left\{ \begin{array}{l} U_z = \pi z \cos\left(\frac{1}{2}\pi r^2\right) \\ \Omega = \pi^2 z r \sin\left(\frac{1}{2}\pi r^2\right) \end{array} \right. \quad (16)$$

$$\left\{ \begin{array}{l} \Omega = \pi^2 z r \sin\left(\frac{1}{2}\pi r^2\right) \end{array} \right. \quad (17)$$

In regions with turbulence, the axial velocity profile deepens as in a typical pipe flow, although in the rocket motor flow the profile changes are due mainly to compressibility corrections. Since the unsteady rotational effects damp rapidly when turbulence is present, no attempt is made here to correct for the changes in the mean flow profile

The complete solution to Eq. (10) is most readily constructed by recognizing that there are two types of oscillatory behavior involved. The first type is related to the acoustic interaction terms on the right hand side. These vary slowly with position like the product of the mean vorticity with the acoustic pressure or velocity. The second type of vortical motion involves rapid variations in the radial direction due to the production of vorticity waves as will be demonstrated shortly. Hence, it is useful to separate the two types of behavior by writing

$$\omega' = \hat{\omega} + \tilde{\omega} \quad (18)$$

where the notation is consistent with that introduced earlier. This allows Eq. (8) to be separated into two independent parts:

$$\left\{ \begin{array}{l} ik_m \hat{\omega} = M_b \left[ik_m p' \Omega + \hat{w} \frac{\partial \Omega}{\partial z} \right] \\ \frac{\partial \tilde{\omega}}{\partial r} + \frac{U_z}{U_r} \frac{\partial \tilde{\omega}}{\partial z} - \frac{\tilde{\omega}}{r} - i \frac{k_m}{M_b U_r} \tilde{\omega} = \frac{1}{M_b U_r} \left[\delta^2 \left(\frac{\partial^2 \tilde{\omega}}{\partial r^2} + \frac{1}{r} \frac{\partial \tilde{\omega}}{\partial r} - \frac{\tilde{\omega}}{r^2} + \frac{\partial^2 \tilde{\omega}}{\partial z^2} \right) + \right. \\ \left. - \frac{\partial \delta^2}{\partial z} \left(\frac{4}{3} \frac{\partial \omega'}{\partial z} - \frac{\partial \omega'}{\partial r} \right) + \right. \\ \left. + \frac{\partial \delta^2}{\partial r} \left(r \frac{\partial \omega'}{\partial r} + \frac{\omega'}{r} \right) + \right. \\ \left. + \frac{\partial^2 \delta^2}{\partial r \partial z} \omega' - \frac{\partial^2 \delta^2}{\partial z^2} \omega' - M_b \frac{\partial \Omega}{\partial z} \tilde{w} \right] \end{array} \right. \quad (19)$$

Terms involving the radial velocity fluctuation in Eq. (10) have been dropped since they introduce terms of only second-order in M_b . The rotational part, Eq. (10), has been written in wave equation form by dividing through by the radial steady velocity at the surface, $M_b U_r$.

The solution of Eq. (19) is straightforward. For a cylindrical chamber the result is

$$\hat{\omega} = \frac{M_b}{k_m} \pi^2 r \sin\left(\frac{1}{2}\pi r^2\right) (k_m z \cos(k_m z) + \sin(k_m z)) \quad (21)$$

for the small part of the vorticity due to interaction of the mean flow with the irrotational unsteady field.

Solution of Eq. (20) for the rotational part is more involved. It is useful to note first that Eq. (20) is a perturbed first-order wave equation.¹⁴ This suggests application of the *ansatz*

$$\begin{cases} \tilde{\omega} = \zeta \exp(i\psi(r)) \sin\left[k_m z \sin\left(\frac{1}{2}\pi r^2\right)\right] \\ \tilde{w} = W \exp(i\psi(r)) \sin\left[k_m z \sin\left(\frac{1}{2}\pi r^2\right)\right] \end{cases} \quad (22)$$

$$\quad (23)$$

where $\zeta(r)$ and $W(r)$ are functions of radial position to be determined. The sinusoidal factor containing the axial position dependence is based on the $\chi(r,z)$ factor of Reference 8, which was expressed in series form as

$$\chi(r,z) = (k_m z) \sum_{j=0}^{\infty} \frac{(-1)^j}{(2j+1)!} (k_m z)^{2j} \sin^{2j}\left(\frac{1}{2}\pi r^2\right) \quad (24)$$

This series can be expressed in closed form¹⁰ as

$$\chi(r,z) = \left[\sin\left(\frac{1}{2}\pi r^2\right)\right]^{-1} \sin\left[k_m z \sin\left(\frac{1}{2}\pi r^2\right)\right] \quad (25)$$

showing the origin of the factor used in the trial solutions of Eqs. (22) and (23). The exponential argument

$$\psi(r) = -\frac{k_m}{\pi M_b} \ln \tan\left(\frac{1}{4}\pi r^2\right) \quad (26)$$

is also based on the findings of Reference 1.

Inserting Eqs. (16) and (17) into (14) and simplifying yields a first-order differential equation for $\zeta(r)$:

$$\frac{\partial \zeta}{\partial r} + i\zeta \frac{d\psi}{dr} - \frac{\zeta}{r} - i \frac{k_m}{M_b U_r} \zeta + \frac{\delta^2}{M_b U_r} \zeta \left(\frac{d\psi}{dr}\right)^2 + \frac{\partial \Omega}{\partial z} \frac{W}{U_r} = 0 \quad (21)$$

where only the significant terms have been retained. For example, the only part of the viscous force that affects the solution is that part arising from the second derivative of ζ with respect to r in Eq. (14). When this second derivative is evaluated, it happens that only the part involving the square of the derivative of ψ gives rise to a significant influence on the solution. That is

$$\frac{d\psi}{dr} = \frac{k_m}{M_b U_r} \quad (22)$$

is inversely proportional to the (small) mean flow Mach number. Hence the square of this term dominates the viscous force as indicated in Eq. (21).

The axial momentum equation (z -component of Eq. (1)) can be used to express function $W(r)$, (which is required to complete the solution of Eq. (21), in terms of the vorticity. One finds

$$ik_m \tilde{w} = M_b \left[\frac{\partial}{\partial z} (U_z w') - U_r \omega' \right] + \delta^2 \frac{1}{r} \frac{\partial}{\partial r} (r \omega') \quad (23)$$

where the radial velocity terms have been omitted as before since they would introduce corrections of second-order in the mean Mach number. Using Eqs. (16) and (17), the axial vortical velocity function is

$$W = i \left(\frac{M_b}{k_m} U_r - i \frac{\delta^2}{M_b U_r} \right) \zeta \quad (24)$$

to good approximation. Substituting this result yields the first-order differential equation for

the vorticity function

$$\frac{d\zeta}{dr} + \left(\frac{\xi}{U_r^3} - \frac{1}{r} - \pi^2 \xi \frac{r^2}{S^2 U_r} - i \frac{\pi^2}{S} r^2 U_r \right) \zeta = 0 \quad (25)$$

where the first term in the brackets is the damping effect due to viscosity. The solution is controlled by two dimensionless parameters, the Strouhal number

$$S = \frac{k_m}{M_b} \quad (26)$$

and the viscosity parameter

$$\xi = \frac{k_m^2 \delta^2}{M_b^3} = \frac{S^2 \delta^2}{M_b} = \frac{S^2}{R_i} \quad (27)$$

which is a combination of the acoustic Reynolds number, Strouhal number, and mean flow Mach number. Table 1 shows values of these key parameters for typical rocket motor configurations.

Table 1. Physical Parameters for Typical Motor Systems

	L (m)	R (m)	M_b	δ	k_m (First mode)	S (First mode)	ξ (First Mode)
Small Research Motor (Yang and Culick ⁷)	0.60	0.025	1.7 ⁻³	5.49 ⁻⁴	1.33 ⁻¹	76.87	1.0309
Tactical Rocket (Typical Geometry)	2.03	0.102	3.1 ⁻³	2.74 ⁻⁴	1.58 ⁻¹	50.84	0.0624
Cold Flow Experiment (Shaeffer and Brown ¹¹)	1.73	0.051	3.3 ⁻³	6.07 ⁻⁴	9.24 ⁻²	28.30	0.0909
Space Shuttle SRM	35.10	0.70	2.3 ⁻³	1.04 ⁻⁴	6.27 ⁻²	27.24	0.0035

Values for the viscous parameter shown in the table are the laminar values applicable in the near vicinity of the burning surface. These correspond to high values of the Reynolds number (typically $Ri > 5000$). As distance from the surface increases and the flow becomes increasingly turbulent, this reference Reynolds number becomes smaller indicating that viscous damping of the vortical waves becomes more important than in the laminar case.

Equation (25) is readily solved by simple quadrature. One finds

$$\zeta = rC \exp(\phi) \quad (28)$$

where the complex coefficient C must be found from the boundary condition expressed Eq. (4). The complex argument $\phi(r)$ arises in the integration of the right side of Eq. (25). Part of the integration cannot be carried out in finite form, since it involves the integral

$$I(r) = \int \frac{x}{\sin(x)} dx \quad (29)$$

which can be represented by the infinite series

$$I(r) = x + \sum_{k=1}^{\infty} (-1)^{k+1} \frac{2(2^{2k-1} - 1)}{(1+2k)(2k)!} B_{2k} x^{1+2k} = x + \frac{x^3}{18} + \frac{7x^5}{1800} + \frac{31x^7}{105840} + \frac{127x^9}{5443200} + \dots \quad (30)$$

Where

$$x = \frac{1}{2} \pi r^2 \quad (31)$$

Functions B_{2k} are the Bernoulli numbers ($B_2 = 1/6$, $B_4 = -1/30$, etc.).

The remainder of the integration is straightforward, and one finds for the real and imaginary parts of ϕ

$$\left\{ \begin{array}{l} \phi^{(r)} = \frac{\xi}{\pi^2} \left[1 - \frac{\pi r^2 \cos\left(\frac{1}{2} \pi r^2\right)}{2 \sin^2\left(\frac{1}{2} \pi r^2\right)} - \frac{1}{\sin\left(\frac{1}{2} \pi r^2\right)} + \left(1 - \frac{2\pi^2}{S^2}\right) (I(r) - I(1)) \right] \end{array} \right. \quad (32)$$

$$\left\{ \begin{array}{l} \phi^{(i)} = \frac{\pi}{S} \cos\left(\frac{1}{2} \pi r^2\right) \end{array} \right. \quad (33)$$

Since this represents the effects of viscous damping of the vorticity wave, it shows that the frictional effect grows rapidly larger as the chamber axis of symmetry is approached. This is both because the vorticity wavelength becomes shorter (spatial frequency becomes higher) and the effective viscosity (eddy viscosity) rapidly increases if turbulence is present. The local axial velocity gradient becomes steeper as r becomes smaller, and the viscous forces become correspondingly more important.

Finally, the vorticity can be written as

$$\tilde{\omega} = C r \exp(\phi + i\psi) \sin\left[k_m z \sin\left(\frac{1}{2} \pi r^2\right)\right] \quad (34)$$

where the complex constant of integration must be

$$C = \frac{S^3 \left((S^2 + \xi) + iS\xi \right)}{\left[(S^2 + \xi)^2 + (S\xi)^2 \right]} \quad (35)$$

Figure 1 shows vorticity vs radial position for a typical tactical rocket motor configuration when no turbulence is accounted for. Notice that while the acoustic mode amplitude is symmetrical fore and aft, the vorticity is not. This reflects the influence of the increasing mean velocity and vorticity in the z -direction.

Since vorticity transport is also a major feature of the turbulent field, it will be of considerable interest to determine what the relationship between the organized vorticity production just described and the turbulent part. That is, when the part of the field dominated by turbulent motions encroaches on the boundary zone in which the organized vorticity originates, it would appear that the role of the shear layer oscillations must be modified. Vorticity produced at the surface will then be transported mainly by the random fluctuations due to the enhanced transport mechanisms associated with the turbulent field. Then the organized shear layer oscillations should be rapidly damped as the gas particles produced in the burning zone move into the chamber.

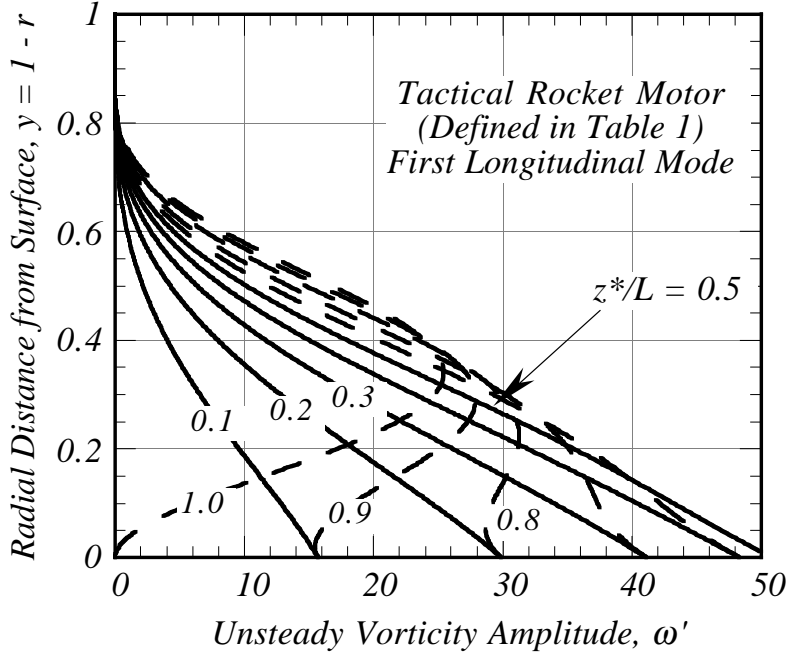


Fig. 1 Laminar Vorticity Distribution, ω' vs. y .

Rotational Velocity Vector Corrections

It is now possible to complete the solution for the unsteady velocity field. The axial component is found by inserting the expressions for ζ from Eq. (28) and $W(r)$ from Eq. (24) into Eq. (17). The result is

$$\tilde{w} = iB r \exp(\phi + i\psi) \sin\left[k_m z \sin\left(\frac{1}{2}\pi r^2\right)\right] \quad (36)$$

where

$$\begin{cases} B^{(r)} = \frac{C^{(r)}}{S} U_r + \frac{\xi}{S^2} \frac{C^{(i)}}{U_r} \\ B^{(i)} = \frac{C^{(i)}}{S} U_r - \frac{\xi}{S^2} \frac{C^{(r)}}{U_r} \end{cases} \quad (37)$$

$$\quad (38)$$

Figure 2(a) shows the composite axial fluctuating velocity ($w' = \hat{w} + \tilde{w}$) and Fig. 2(b) the corresponding phase angle vs. radial position for a typical case if no effects of turbulence are accounted for.

It remains to determine the radial velocity correction resulting from the production of vorticity. This velocity must be added to whatever surface fluctuation is present due, for example, to pressure or velocity coupled combustion response. It is important to see that this correction is required by continuity since the no-slip condition gives rise to a momentum defect at the surface as in simple boundary layer theory.

In the present case, the continuity equation that must be satisfied by the rotational part of the unsteady flow is

$$\frac{1}{r} \frac{\partial}{\partial r} (r\tilde{u}) + \frac{\partial \tilde{w}}{\partial z} = 0 \quad (39)$$

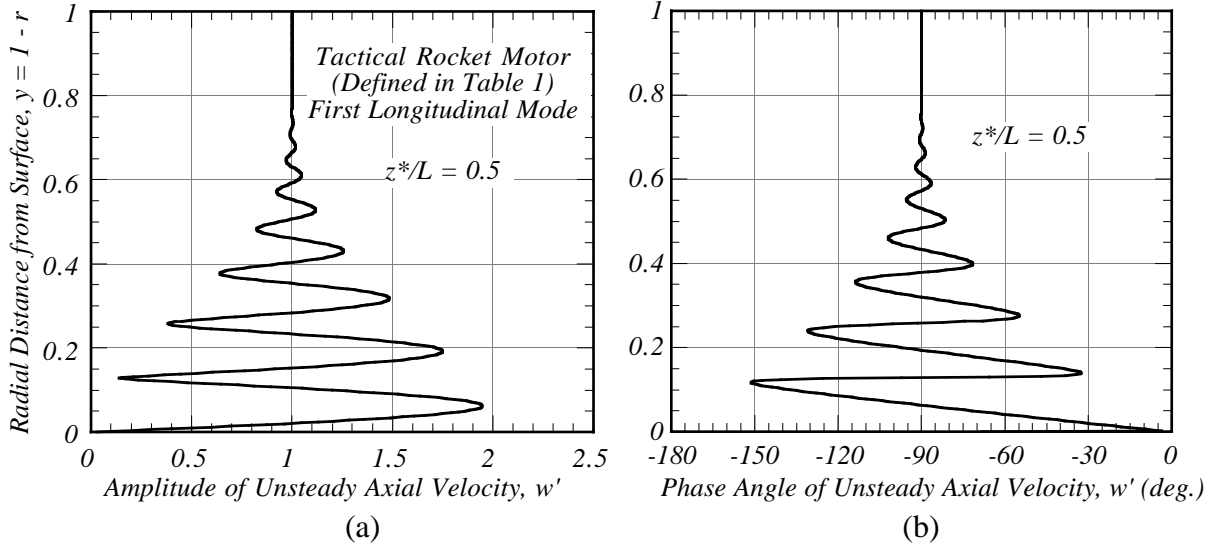


Fig. 2 Laminar Axial Velocity Amplitude and Phase Angle vs. y .

The radial velocity can be found directly by setting

$$\tilde{r}u = f(r)\exp(\phi + i\psi)\cos\left[k_m z \sin\left(\frac{1}{2}\pi r^2\right)\right] \quad (40)$$

and using Eq. (36) to represent the axial component. This yields

$$\tilde{u} = M_b Br^2 U_r^2 \exp(\phi + i\psi)\cos\left[k_m z \sin\left(\frac{1}{2}\pi r^2\right)\right] \quad (41)$$

where negligible terms (of order M_b^2) are not shown.

It is important to observe that this radial velocity fluctuation does not vanish at the burning surface. At $r = 1$, one finds for the real part

$$\tilde{u}^{(r)} = -M_b \left(\frac{S^2(S^2 + \xi) + \xi^2 S^2}{(S^2 + \xi)^2 + (S\xi)^2} \right) \cos(k_m z) \approx -M_b \cos(k_m z) \quad (42)$$

where the approximate result corresponds to cases for ξ/S small, which it is in most realistic situations since the flow behavior is nearly laminar in the viscous sublayer.

The surface radial velocity correction must be carefully accounted for in the motor stability calculations and in construction solutions for the gas motions in the combustion zone. Most work on this problem has been based on the assumption of one-dimensional flow normal to the surface. This seems justifiable on the basis of the thinness of the combustion layer. However, as will be demonstrated in what follows, there are strong effects due to parallel wave influence that are eliminated by this and related assumptions (quasi-steady, one dimensional gas phase). Past failure to demonstrate a consistent model for velocity coupling is also related to this set of limiting assumptions.

Effects of Turbulence on Organized Unsteady Flow

It is clear that in real motor chambers there will be two types of unsteady motion when the field is both turbulent and supports acoustic waves (and the associated vortical waves originating at the inflow boundaries). It is necessary to determine how turbulence will affect the organized wave motions. The laminar solution described in the last subsections will be extended by introducing numerically determined turbulent transport properties. As already indicated this is an approximate method for accounting for turbulent effects and does not include direct turbulent flow interactions with the organized wave motions.

Calculations for the development of the turbulent field were carried out for all of the typical motor geometries described in Table 1. For example, Figure 3 shows the evolution of turbulence intensity plotted vs radial position as a function of axial position ($z/L = 1$ corresponds to the nozzle end of the chamber). The turbulence intensity is zero at the chamber axis and peaks at a position which is typically within 1/10 the chamber radius from the burning surface. The turbulent intensity grows in magnitude rapidly as the nozzle end is approached.

Figure 4 shows the axial velocity profile for the tactical motor configuration indicating transition to a turbulent profile as distance along the chamber increases. The Culick mean flow profile is reproduced for axial positions less than about $z/L = 0.3$. The profile deepens as turbulence further dominates the field with increasing axial distance from the chamber head-end. This is consistent with the usual turbulent pipe flow computations. The turbulent axial velocity profiles near the nozzle end can be fit quite closely with universal pipe flow turbulent profiles such as those devised by Von Karman.

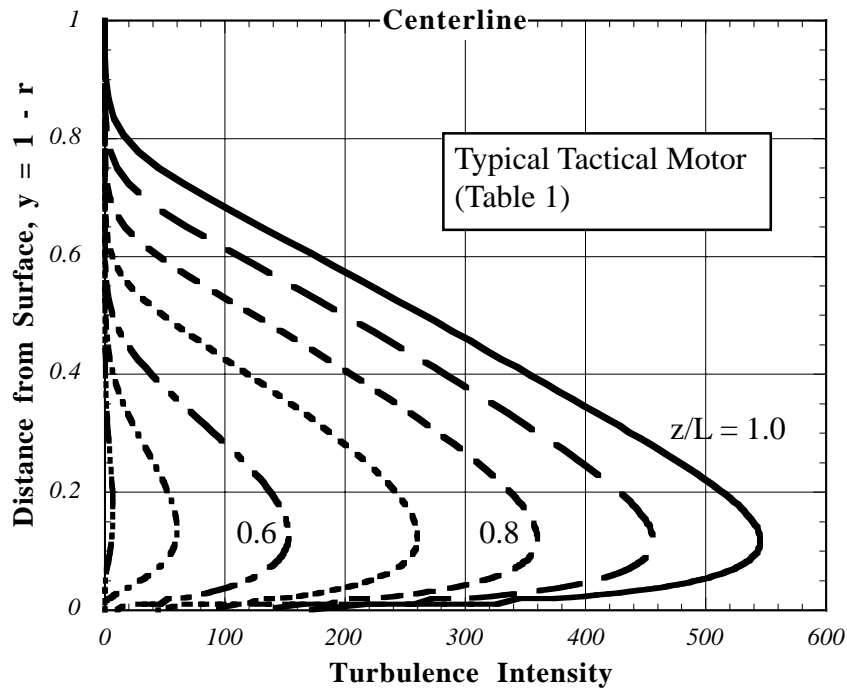


Fig. 3 Turbulence Intensity Distribution.

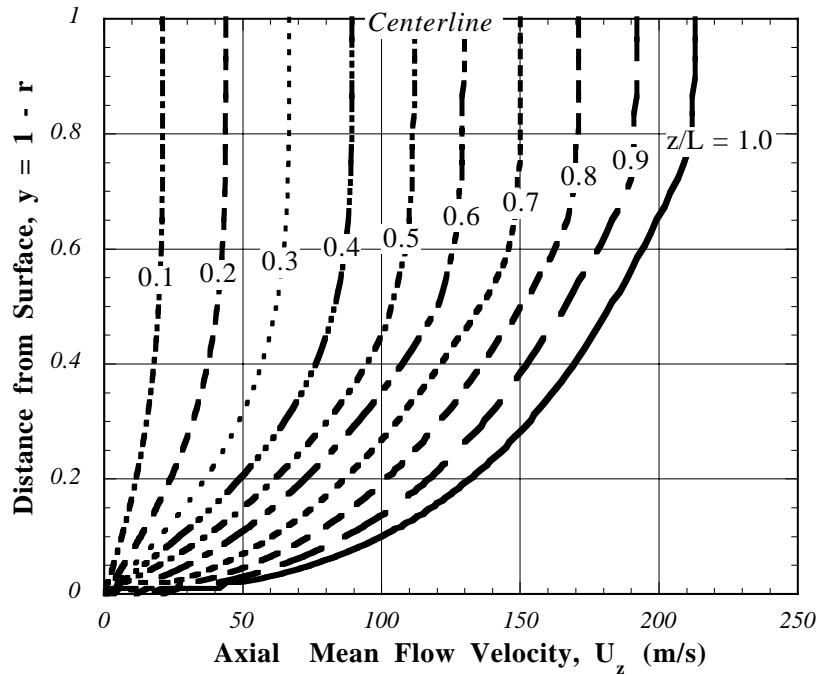


Fig. 4 Effect of Turbulence on Axial Mean Flow Velocity Profile.

Figure 5 is a plot of the turbulent eddy viscosity distribution as a function of position within the motor. This transport property has a major influence on the organized wave structures, since they are strongly dependent on viscous dissipation. Near the surface, within the laminar sublayer, the laminar solutions are assumed to hold. That is the molecular viscosity dominates the unsteady flow. As distance from the burning surface increases, the effects of turbulent transport becomes rapidly more important, and dissipation of the energy contained in the organized rotational flow occurs far more rapidly than in the laminar case.

The turbulent transport properties can be used in the expressions developed for the organized unsteady gas motions to approximate the effects of turbulence on the wave structure. The laminar behavior described in Figure 2 is only maintained near the chamber forward end. As the turbulence dominates the chamber flow as axial distance increases, the laminar motion is replaced by the turbulent organized oscillations.

Figure 6 shows the development of the longitudinal oscillations with axial position. Results shown are for a first mode longitudinal oscillation in the Shuttle SRM. Smaller motors show a more rapid transition to a turbulence-modified solution. The rotational flow effects penetrate deeply into the chamber near the forward end, but rapidly transition to a turbulent form as z/L increases. The turbulent form of the motion closely resembles a typical acoustic boundary layer in which the rotational flow corrections to the longitudinal acoustic wave are confined to a thin zone near the surface. As the nozzle is approached, this effect is enhanced, and it can be seen that this can be thought of as the unsteady analog to the erosive burning situation. In this case, the axial unsteady velocity profiles are deepened in the burning zone. It remains for later study to determine how these changes affect the unsteady combustion characteristics, and in particular, the response function of the combustion layer.

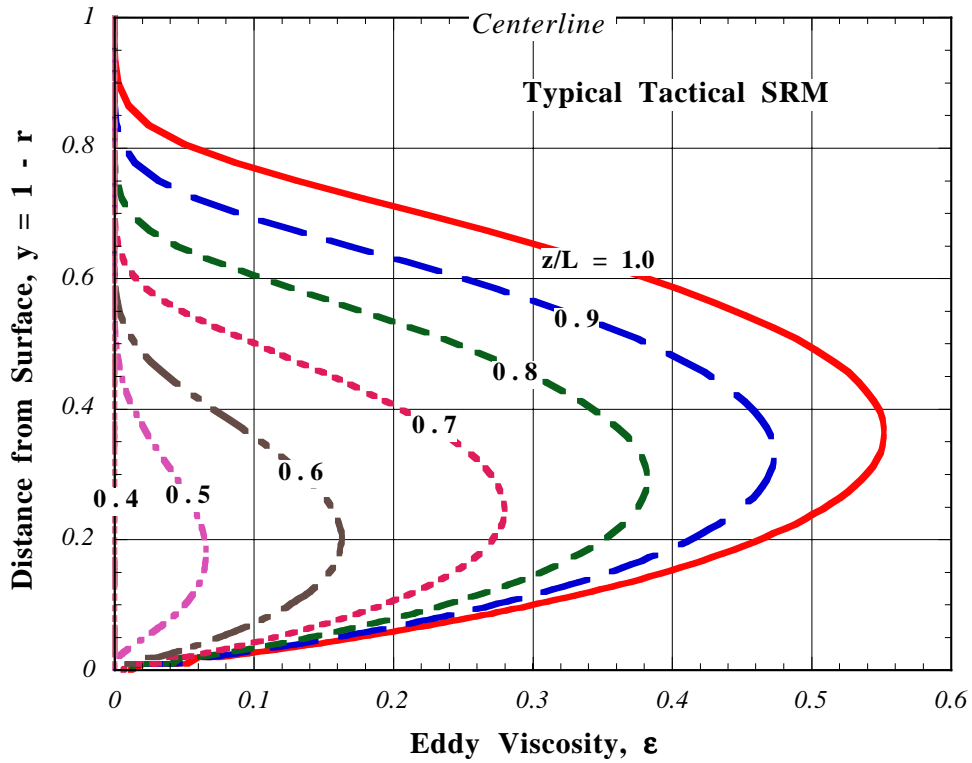


Fig. 5 Eddy Viscosity Distribution in Typical Tactical Rocket.

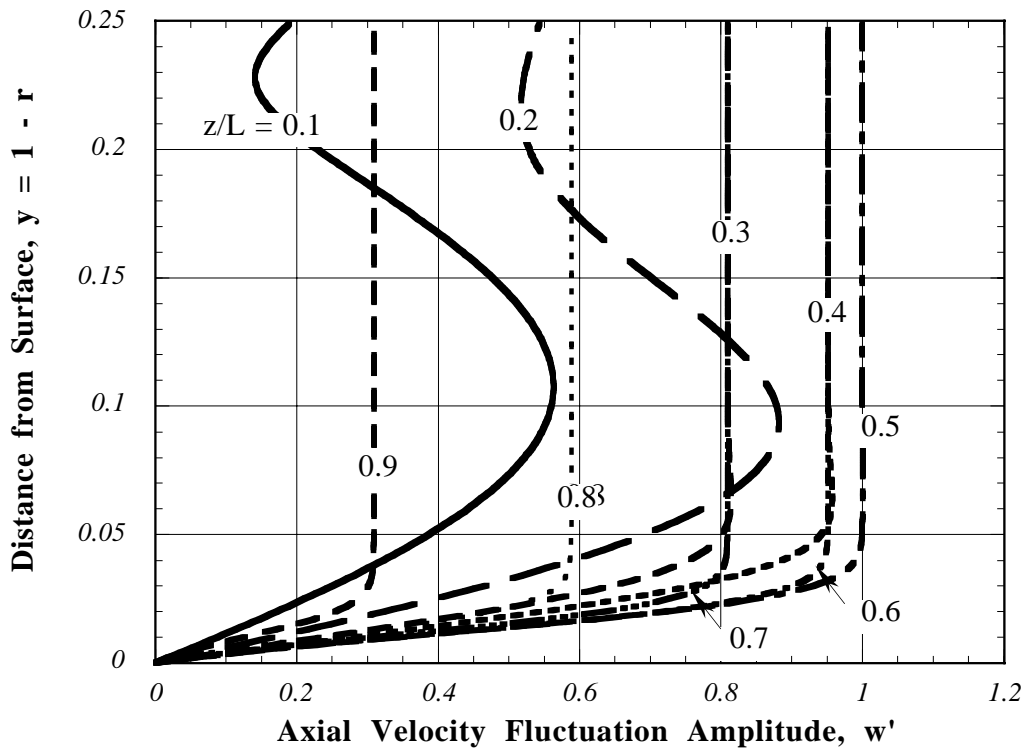


Fig. 6. Effect of Turbulence on Axial Wave Amplitude (Shuttle SRM).

To see the strong turbulence interaction with the surface rotational waves, compare the plots for w' in Figure 6 at a position 1/10 of the chamber length from the head-end showing the typical laminar behavior and that at 9/10 of the length showing the turbulent behavior. The large overshoot is eliminated, and the profile more closely resembles a classical acoustic boundary layer. It remains to determine the consequences of these changes have on key stability calculations.

Effect of Turbulence on Vorticity Production and Transport

We have already demonstrated the important role played by vorticity in accommodating the principal wave motion (assumed to be a longitudinal plane acoustic wave) to the necessary no-slip boundary conditions. In the absence of turbulence, vorticity is produced at the surface and transported as a rotational wave or shear wave as illustrated in Figure 2. When turbulence is present, the mechanism for vorticity transport is changed because of the enhanced turbulent transport. It is of interest to test the present model to determine if it demonstrates these expected features. Figure 7 compares the laminar and turbulent solutions at a point somewhat less than a third the chamber length from the forward closure. At this location, the turbulent flow has not yet reached a dominant level, and there is only a small difference in the organized vorticity amplitude distribution.

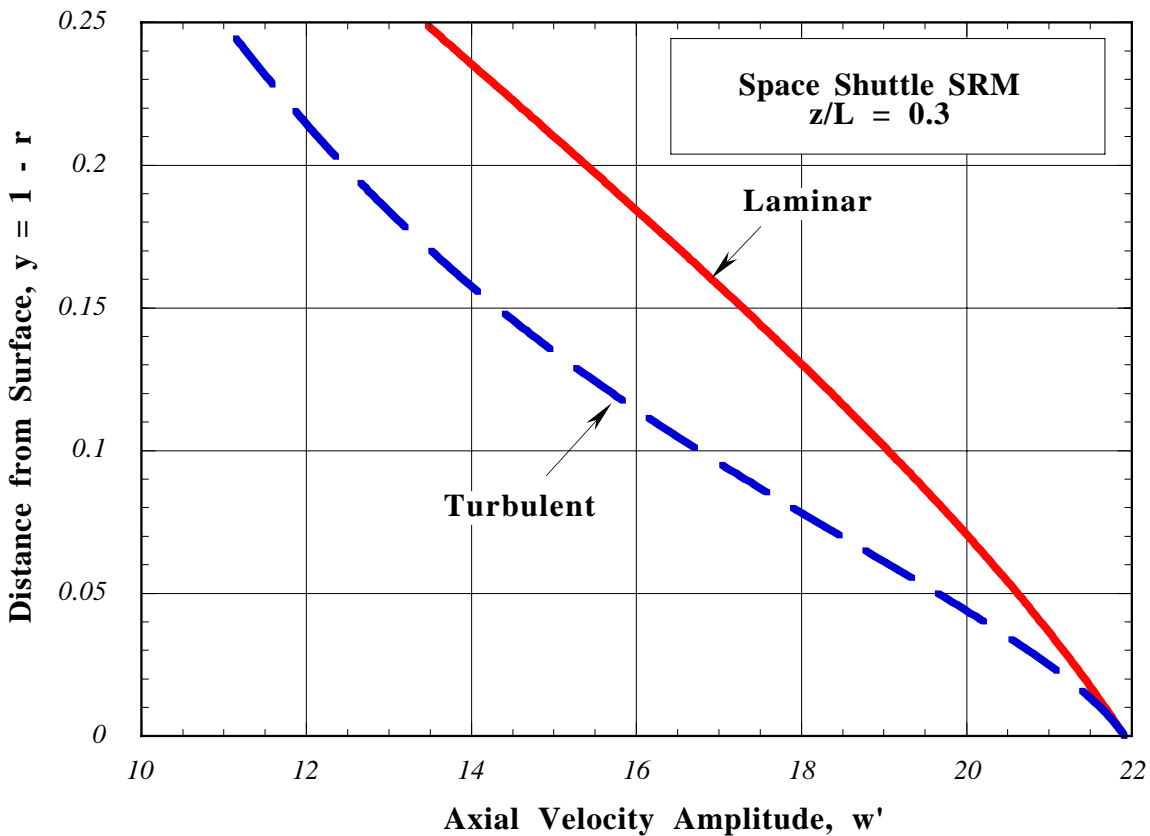


Fig. 7. Effect of Turbulence on Organized Vorticity Distribution (Shuttle SRM).

As the axial distance increases, the turbulent motion begins to dominate the field. At the location $z/L = 0.4$, only slightly downstream of the position illustrated in Figure 7, a major modification in the organized unsteady field is apparent. As shown in Figure 8, the turbulent fluctuations greatly modify the vorticity distribution indicating the random motions have taken over in transporting the vorticity produced at the wall into the interior of the chamber. Notice that there is no change in the magnitude of the vorticity at the surface since this is determined entirely by the pressure gradient across the incoming streamlines. The behavior near the surface is reminiscent of a *laminar sublayer*. The laminar and turbulent solutions are coincident near the inflow boundary.

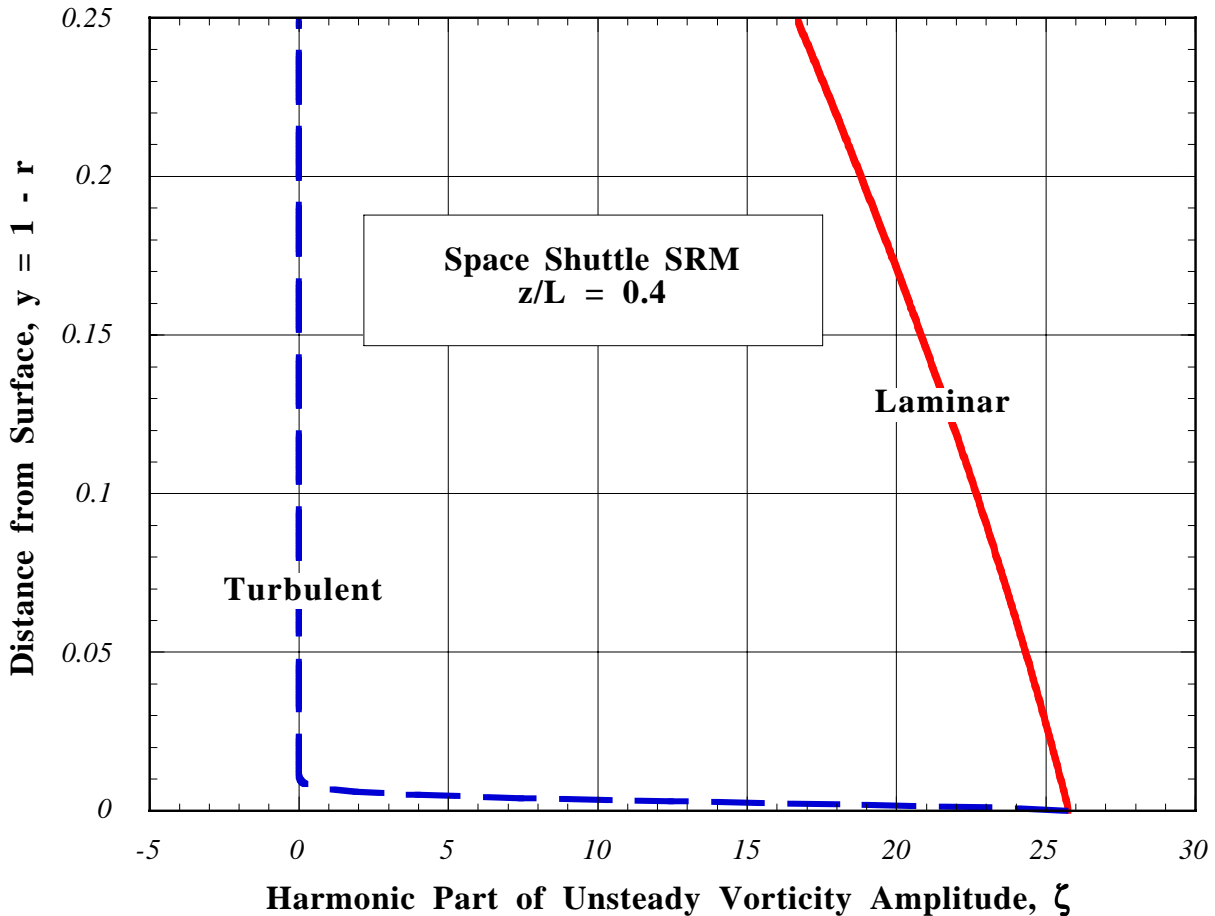


Fig. 8. Effect of Turbulence on Organized Vorticity Distribution (Shuttle SRM).

Effect of Turbulence on System Stability Integrals

In estimating the tendency for a given motor to exhibit linear instability, it is necessary to account for many loss/gain effects in determining the net growth rate of an acoustic wave. A very important element is the flow-turning damping term identified by Culick. The original form of this damping effect was deduced in a one-dimensional calculation. It appeared because the no-slip boundary condition was invoked at the lateral burning surfaces. There followed many years of confusion, since this term did not appear in the standard multidimensional stability model. It was demonstrated in Reference 1 that the classical flow-turning loss is the one-dimensional equivalent of the volume integral

$$\alpha_{FT_1} = -\frac{M_b}{2k_m E_m^2} \oint \iiint_V (\mathbf{U} \times \boldsymbol{\omega}') \cdot \nabla p'_m dV \quad (43)$$

where

$$E_m^2 = \iiint_V (p'_m)^2 dV = \frac{\pi L}{2R} \quad (44)$$

is the dimensionless normalization function, evaluated here for a cylindrical chamber with an axial acoustic wave. The first term, Eq. (43), can be written as a surface integral since

$$\boldsymbol{\omega}' = \frac{\partial u'}{\partial z} - \frac{\partial w'}{\partial r} \approx -\frac{\partial w'}{\partial r} \quad (45)$$

The approximate form is valid since the radial velocity fluctuation is small ($O(M_b)$) and changes only slowly with respect to z . Figure 8 suggests that both laminar and turbulent results are the same at the surface where the stability integral must be evaluated. Also, the integrand in Eq. (43) oscillates rapidly to zero at the centerline ($r = 0$). Therefore, the value of the volume integral is determined entirely by its upper limit (at $r = 1$). The integrand near the upper limit can therefore be accurately represented as

$$(\mathbf{U} \times \boldsymbol{\omega}') \cdot \nabla p'_m = -k_m \frac{\partial \tilde{w}}{\partial r} \sin(k_m z) = \frac{\partial}{\partial r} (\tilde{\mathbf{u}} \cdot \nabla p'_m) \quad (46)$$

since the derivative of the vortical velocity with respect to r dominates. This is because $\tilde{\mathbf{u}}$ involves ψ , whose derivative is proportional to the inverse of the mean flow Mach number as shown in Eq. (22). Then the flow turning integral reduces to the surface integral

$$\alpha_{FT} = -\frac{1}{2E_m^2} \iint_{S_b} \left(\frac{M_b}{k_m} \tilde{\mathbf{u}}^{(i)} \cdot \nabla p'_m \right) dS_b \quad (47)$$

where the integration is over the burning surface. Notice that only the rotational part of the velocity fluctuation is involved in the flow-turning integral. Therefore, the flow-turning stability correction vanishes if one assumes an irrotational unsteady flow as was done in formulating the three-dimensional stability algorithm now in widespread use. Equation (47) is the correct three-dimensional form for the flow-turning effect and it is now being incorporated in updated versions of the Standard Stability Prediction code. Of considerable importance is the demonstration given here that this result is not affected by turbulence. This is the result of the independence of this damping effect from viscous processes. It represents the energy loss incurred in the process of transfer of energy from the pressure oscillations (acoustic field) into the complete chamber unsteady flow field.

There are other surface effects that influence the system stability that are related to satisfying the no-slip boundary condition at the combustion boundary. These results are discussed in Reference 1, and will not be repeated here. Let it suffice to say that modifications in the fluctuating velocity normal to the surface brought about by rotational flow effects must be accounted for in motor stability computations. What has been demonstrated in the present work is that these are not affected by the encroachment of turbulence on the inflow boundaries; related modifications to the combustion response function are currently being evaluated. This is not to say that the turbulent modifications do not affect the combustion in other ways.

Conclusions

A fully analytical solution to the Navier-Stokes equations describing the unsteady flow in a cylindrical chamber with sidewall injection has been used in this paper to establish the effects of viscosity on the flow-turning effect in rocket motor combustion instability when strong turbulence is present. The turbulence features are evaluated numerically and the resulting modifications to the chamber transport properties are used in evaluating the analytical expressions describing the unsteady vorticity and velocity distributions.

The results support the findings of earlier fully numerical studies by Yang and his coworkers¹⁻², which indicated that there is a major influence of turbulence on the unsteady flow features near the combustion zone. The benefits of the present analytical approach are

- Enhances physical understanding of the flow processes near the combustion zone
- Allows ready evaluation of the system linear stability properties in a manner consistent with established stability algorithms
- Provides methods that will be useful in further improvement in modeling of the combustion zone in the presence of turbulent fluctuations.

The organized gas oscillations near the burning surface are controlled by two scaling parameters. These are the Strouhal number, S , based on the acoustic frequency and the injection velocity at the propellant surface, and the injection Reynolds number, R_i . When turbulence is present, the viscous effects are enhanced. There is an apparent decrease in the effective Reynolds number. Then the organized shear waves are rapidly damped and vorticity transport is dominated by turbulent gas motions.

The results demonstrate that the flow-turning can be conveniently represented by a simple surface integral over the chamber boundaries in keeping with other main elements of the stability assessment algorithm. It is demonstrated that turbulence does not modify this result and other related stability affects related to production of vorticity at the chamber inflow boundary.

These stability results are virtually independent of viscosity, although viscous forces greatly influence the unsteady velocity distributions in the volume of the combustion chamber. This is a consequence of the fact that viscous forces are negligible near the injection surface in the laminar sublayer. They are enormously enhanced in strongly turbulent regions because of the modifications to the gas transport properties.

Acknowledgment

This work was sponsored partly by the Pennsylvania State University and the University of Tennessee (UTSI) and partly by California Institute of Technology Multidisciplinary University Research Initiative under ONR Grant No. N00014-95-1-1338, Program Manager Dr. Judah Goldwasser.

Nomenclature

A_b	Pressure coupling admittance function
A_v	Velocity coupling admittance function
a_0	Mean speed of sound
$\mathbf{e}_r, \mathbf{e}_\theta, \mathbf{e}_z$	Unit vectors in r , θ , and z directions
E_m^2	Normalization constant for mode m
k_m	Wave number for axial mode m
L	Chamber length
m	Mode number
M_b	Mach number at burning surface
\mathbf{n}	Outward pointing unit normal vector
p	Pressure
P_0	Mean chamber pressure
r	Radial position
R	Chamber radius
$S = k_m/M_b$	Strouhal Number
t	Time
\mathbf{t}	Unit vector tangent to burning surface
\mathbf{u}'	Oscillatory velocity vector amplitude
U_r, U_z	Mean flow velocity components
u, w	Unsteady flow velocity components
y	Radial position ($y = 1 - r$)
z	Axial position
α	Growth rate (dimensional, sec^{-1})
$\lambda = M_b/k_m$	Inverse of Strouhal number
ν	Kinematic viscosity ($\nu = \mu/\rho$)
ρ	Density
ψ	Complex exponential argument
ω'	Amplitude of vorticity fluctuation
Ω	Mean vorticity amplitude
Ω_b	Vorticity amplitude at burning surface

Subscripts

b	Combustion zone
m	Mode
0	Zeroth order in M_b
$\underline{1}$	First order in M_b
t	Tangential part
n	Normal part

Superscripts

*	Dimensional quantity
(1)	First order in wave amplitude
'	Amplitude of time-dependent part

References

1. Cai, W. and Yang, V., "Two-Phase Turbulent Flow Interactions in a Simulated Rocket Motor with Acoustic Waves," AIAA paper 98-0161, *36th Aerospace Sciences Meeting & Exhibit*, Reno, 1998.
2. Rodi, W. "Experience with Two-Layer Models Combining the k - ϵ model with One-Equation Model near the wall," AIAA Paper No. 91-0216, Jan. 1991.
3. Wilcox, D. C., "Turbulence Modeling for CFD," *DCW Industries, Inc. La Canada, California*, 1993.
4. Yam, C., and Dwyer, H. "Investigation of the Influence of Blowing and Combustion on Turbulent Wall Boundary Layers," *AIAA Journal*, Vol. 27, No. 3, 1989, pp. 370-371.
5. Gibeling, H., "Advanced Flow Field Model," PL-TR-93-3005 Mar. 1993, pp. 24-27.
6. Kays, W. "Heat Transfer to the Transpired Turbulent Boundary Layer," *J. Heat Mass Transfer*, Vol.15, 1972, pp. 1023-1044.
7. Tseng, I-Shih, Yang, V. "Combustion of a Double-Base Homogeneous Propellant in a Rocket Motor," *Combustion and Flame* v. 96 n. 4 Mar 1994 pp. 325-342.
8. Cousteix, J, "Investigation of the Structure and of the Development of a Turbulent Boundary Layer in an Oscillating External Flow," Symposium on Turbulent Shear Flows, Pennsylvania State University. Apr.1977.
9. Mizushima, T. "Structure of the Turbulence in Pulsating Pipe Flows," *J. Chem. Eng. Japan*, Vol.8, No.3, 1975.
10. Ramprian, B. R. and Tu, S. W. "An Experimental Study of Oscillatory Pipe Flow at Transitional Reynolds Numbers," *J. Fluid Mech.* Vol.100, No.3, 1980, pp.513-544.
11. Ramprian, B. R. and Tu, S. W. "Fully Developed Periodic Turbulent Pipe Flow, Part2: Detailed Structure of the Flow," *J. Fluid Mech.* Vol.137, 1983, pp.59-81.
12. Fan, S. and Lakshminarayana, B. "Low-Reynolds-Number k - ϵ Model for Unsteady Turbulent Boundary-Layer Flows," *AIAA Journal*, Vol.31, NO.10, Oct. 1993, pp.1777-1784.
13. Kovalnogov, N. "Unsteady Heat Transfer and Friction in Internal Axisymmetric Flows with Longitudinal Pressure Gradients," *Heat Transfer Research*, Vol.25, No.3, 1993, pp.304-307.
14. Flandro, G. A., "Effects of Vorticity on Rocket Combustion Stability," *AIAA J.*, Vol. 22 No.4, July-August 1995.